



Deposited via The University of Leeds.

White Rose Research Online URL for this paper:

<https://eprints.whiterose.ac.uk/id/eprint/182706/>

Version: Supplemental Material

Article:

Porter, AJ, Botchway, C, Kwakye-Awuah, B et al. (2022) Local and Nanoscale Methanol Mobility in Different H-FER Catalysts. *Catalysis Science and Technology*, 12 (5). pp. 1663-1677. ISSN: 2044-4753

<https://doi.org/10.1039/D1CY02001C>

Reuse

Items deposited in White Rose Research Online are protected by copyright, with all rights reserved unless indicated otherwise. They may be downloaded and/or printed for private study, or other acts as permitted by national copyright laws. The publisher or other rights holders may allow further reproduction and re-use of the full text version. This is indicated by the licence information on the White Rose Research Online record for the item.

Takedown

If you consider content in White Rose Research Online to be in breach of UK law, please notify us by emailing eprints@whiterose.ac.uk including the URL of the record and the reason for the withdrawal request.

Local and Nanoscale Methanol Mobility in Different H-FER Catalysts

A.J. Porter^a, C.H. Botchway^{b,c}, B. Kwakye-Awuah^d, C. Hernandez-Tamargo^{ce}, S.K. Matam^{cf}, S. McHugh^a, I. Silverwood^{fg}, N.H. de Leeuw^{ch*}, A.J. O'Malley^{a,f*}

^aCentre for Sustainable and Circular Technologies, Department of Chemistry, University of Bath, BA2 7AY, UK

^bDepartment of Chemistry, Kwame Nkrumah University of Science and Technology, Kumasi 1916, Ghana

^cSchool of Chemistry, Cardiff University, Cardiff CF10 3AT, UK

^dDepartment of Physics, Kwame Nkrumah University of Science and Technology, UPO, PMB, Kumasi, Ghana

^eNational Centre for Catalysis Research, Department of Chemistry, Indian Institute of Technology Madras, Chennai 600 036, India

^fUK Catalysis Hub, Research Complex at Harwell, Science and Technology Facilities Council, Rutherford Appleton Laboratory, Oxford, OX11 0FA, UK

^gISIS Pulsed Neutron and Muon Facility, Science and Technology Facilities Council, Rutherford Appleton Laboratory, Didcot, OX11 0QX, UK

^hSchool of Chemistry, University of Leeds, Leeds LT2 9JT, UK

* n.h.deleeuw@leeds.ac.uk, a.o'malley@bath.ac.uk

Supplementary information

SI 1.0 Zeolite synthesis

Ferrierite (FER) zeolite was synthesized using piperidine as the structure directing agent (SDA) under traditional hydrothermal conditions. Sodium aluminate solution was obtained by digesting 1-liter of 4 M sodium hydroxide (Fischer Scientific, UK) at 150 °C for 8 h. The solution was filtered and refluxed in a water bath after which it was allowed to cool to room temperature. 100 ml of SDA was added to a dealuminated metakaolin slurry (200 g of metakaolin in 200 ml de-ionized water), prepared by leaching with 2 M 98 % sulfuric acid, and added into a Teflon-lined stainless-steel autoclave. The metakaolin was obtained by heating the kaolin samples at 750 °C for 1 hour and cooling in air to 30 °C.

After combining and stirring for 1 h, the mixture was heated under reflux with periodic stirring at 180 °C for 24 hours. The reaction was quenched with water and the crystals were filtered and washed with an excess of de-ionized water until the solution was near neutral. The SDA was removed by calcination at 600 °C for 3 h. To obtain the sodium form of the Ferrierite, 1 M NH₄NO₃ solution was added to the crystallized zeolite at 60 °C for 3 h with stirring. This procedure was repeated twice. The sample was then washed with deionized water three times, dried, and calcined at 550 °C for 3 h to obtain the proton form, H-FER. The product was ground to fine powder.

SI 1.1 MD simulation design and analysis

Below are the details pertaining to the design, construction and analysis of the molecular dynamics simulations including the forcefield, framework construction and trajectory analysis.

Zeolite-Zeolite interactions			
Buckingham Potential			
Atoms	A (eV)	ρ (Å)	C (eV Å⁶)
Si-O	1283.907	0.32052	10.66158
Si-O _b	983.5566	0.32052	10.66158
O-O ^a	22764.0	0.149	27.88
Al-O	1460.3	0.29912	0
Al-O _b	1142.6775	0.29912	0
O-H _b	311.97	0.25	0
Morse Potential			
Atoms	D (eV)	α (Å⁻¹)	r_0 (Å)
O _b -H _b	7.0525	2.1986	0.9845
Three-body Potential			
Atoms	k (eV rad⁻²)	θ (°)	
O-Si-O/O _b	12.1	109.47	
O-Al-O/O _b	2.2	109.47	

^a O-O, O-O_b and O_b-O_b

Table SI1. Potential parameters of the zeolite framework

Charges	
Ion	Charge
C	-0.093
H _c	+0.1
O	-0.432
H _o	+0.225

Methanol intramolecular potentials			
Harmonic Potential			
Atoms	k (eV Å ⁻²)	C (eV Å ⁶)	
C-H	1283.907	10.662	
C-O	1406.3	0	
O-H _o	22764.0	28.92	
Harmonic angle Potential			
Atoms	k (eV rad ⁻²)	θ (°)	
C-O-H _o	5.6	108.32	
H-C-O	5.5	106.90	
H-C-H	4.4	108.38	
Dihedrals			
Atoms	k (eV)	A	β
H-C-O-H _o	0.00762	1.0	3.0

Table SI2. Assigned ionic charges of the methanol atoms in the molecular dynamics simulations and Intramolecular methanol potential parameters

Intermolecular potentials		
Lennard Jones Potential		
Atoms	ε (eV)	σ (Å)
H-H/H _{MeOH}	0.00165	2.450
C-C	0.00694	3.475
H-C	0.00338	2.920
H-O _{MeOH}	0.00404	2.650
O _{MeOH} -O _{MeOH}	0.00988	2.860
O _{MeOH} -C	0.00828	3.150
O _{MeOH} -H _{MeOH}	0.00404	2.650
C-H _{MeOH}	0.00338	2.920
O/O _b -H _{MeOH}	0.004987	2.557
O/O _b -O _{MeOH}	0.010545	2.764
O/O _b -H	0.004987	2.557
O/O _b -C	0.005910	4.310
H _b -H _{MeOH}	0.000851	1.784
H _b -O _{MeOH}	0.00338	2.920
H _b -H	0.000851	1.784
H _b -C	0.00299	2.806

Table SI3. Intermolecular methanol-methanol and zeolite-methanol potential parameters

SI 1.1.1 Framework construction

Each aluminium atom was placed with its associated charge compensating proton protruding into one of the pores. This resulted in one aluminium with its proton in the pore lying perpendicular to the 001 axis and the other with its proton in the pore lying perpendicular to the 010 axis. This enables maximum adsorbate exposure to the Brønsted acid sites – modelling a more extreme scenario in terms of zeolite-methanol interactions. This placement also maintains that they are as far apart as possible, minimising Al-Al interactions, to abide by Dempsey's rule¹ whilst also accounting for the periodic boundary conditions. The Brønsted acid sites were denoted O_b-H_b.

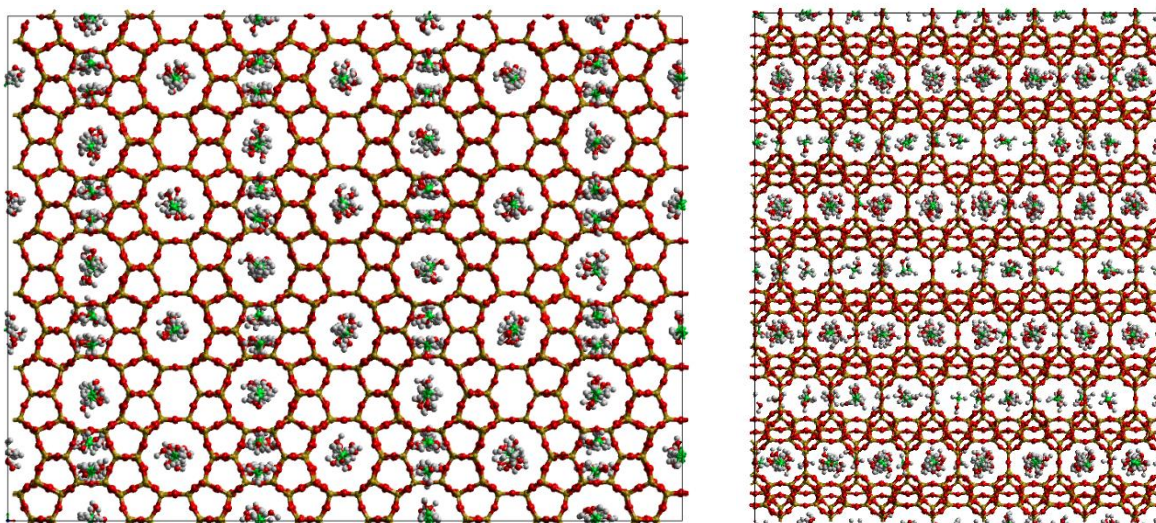


Figure SI1.1. A methanol loaded siliceous FER type zeolite 4 x 4 x 8 supercell production supercell, viewed from the 001 and 010 directions. Silicon (yellow), oxygen (red) and aluminium (blue).

SI 1.2 Mean squared displacement and Method of multiple time origins

The mean squared displacement of the methanol molecule was tracked using the carbon atoms position as opposed to calculating the whole molecules centre of mass at each timestep which would incur an additional computational expense. The difference in diffusivity calculated between these two methods is found to be insignificant with diffusion coefficients for the methanol in the siliceous FER at 300 K found to be $0.89 \pm 0.04 \times 10^{-11} \text{ m}^2\text{s}^{-1}$ when tracking the carbon atom and $0.90 \pm 0.04 \times 10^{-11} \text{ m}^2\text{s}^{-1}$ when tracking the molecules centre of mass.

The method of multiple time origins was used to improve the statistics of each simulation. An MSD plot of the first 1 ns was taken, with further MSDs taken starting at an offset of 1 ps from the origin (i.e. 0-1000 ps, 1-1001 ps, 2-1002 ps, etc) until the whole 2 ns simulation was covered. The average of the resulting one thousand 1 ns MSD plots was then calculated.

SI 1.3 Contact correlation function analysis

The contact correlation function between the methanol molecules and the Brønsted acid sites in the Si/Al ratio = 35 was also calculated, using equation 2:

$$C(t) = \frac{1}{N} \sum_{i=1}^N \frac{\langle p_i(t) \rangle}{\langle n_i(t_0) n_i(t_0) \rangle} \quad (2)$$

Where N is the total number of molecules adsorbed at the initial time t_0 and $p_i(t)$:

$$p_i(t) = n_i(t_0) \prod_{t_0}^t n_i(t) \quad (3)$$

Where $n_i(t)$ is a binary function which equals 1 when the two molecules are within the specified contact distance and 0 when they are not. In this work, the contact distance was defined as 3.0 Å. An average over several time origins – initial times – was calculated. The contact correlation function may be used to define a residence time, t_r :

$$t_r = \int_0^{\infty} dt C(t) \quad (4)$$

The residence time describes the average time period an adsorbate molecule stays bonded to a site. The residence time coincides at $\tau = t_r$ when the contact correlation decays exponentially i.e. $C(t) = e^{-t/\tau}$. t_r thus corresponds to the time at which $C(t) = e^{-1} = 0.3679$.² To achieve a single exponential

function the contact distance must be sufficiently small to only observe behaviour within one coordination sphere. The 3 Å cutoff was reached by decreasing the contact distance until a single exponential is observed. Linear combinations of similar exponential functions may be fit to describe multiple different behaviours over a larger cutoff distance. Once the closest behaviour, within the first coordination sphere, has been sampled, more exponentials may be fit over a larger cutoff however this was not undertaken in this work.

SI 1.4 Zeolite characterisation

The following section contains all of the characterisation of the FER catalyst ‘FER-GHA’ and the commercial FER including the BET, SEM, EDX, neutron diffraction and X-ray diffraction data. The saturation point of the commercial FER sample was found to be 7.34 wt%, with a loading of 6.26 also included. The FER-GHA achieved a loading of 10.18 wt%. One molecule per unit cell (MPUC) equates to a loading of 1.48 wt% - calculation shown in the table below – therefore leading to loadings of ~5 MPUC, ~4 MPUC and ~7 MPUC.

	Number of atoms	Mass of atom(s)
FER unit cell		
Si	36	28.0855
O	72	15.999
	Total A	2163.006
Methanol		
C	1	12.0107
H	4	1.00784
O	1	15.999
	Total B	32.04106
	wt%	100 × (Total B/Total A)
	wt% calculation	1.481

Nitrogen adsorption–desorption isotherms were collected at 77 K on a Quadrasorb EVO instrument (model QDS-30) for both samples – see figure SI1.4.1. Prior to the experiments, the zeolites were outgassed at 473 K for 24 h. The total surface area was determined by the Brunauer–Emmett–Teller (BET) method. The total surface area of the FER-GHA was calculated to be 41 m²/g and 293 m²/g for the commercial FER.

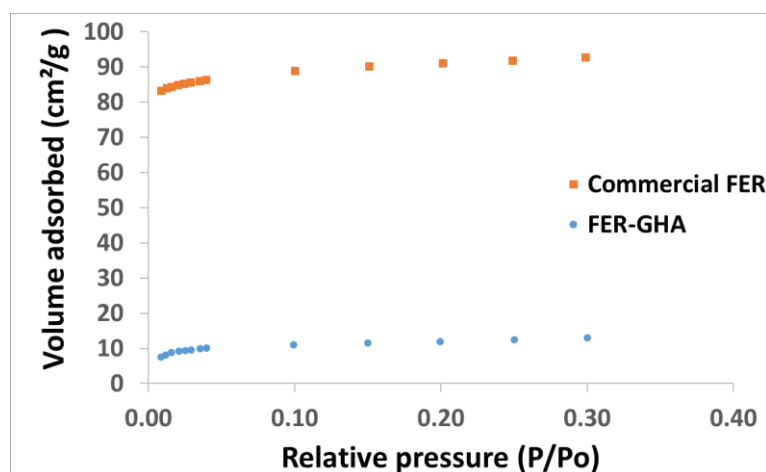


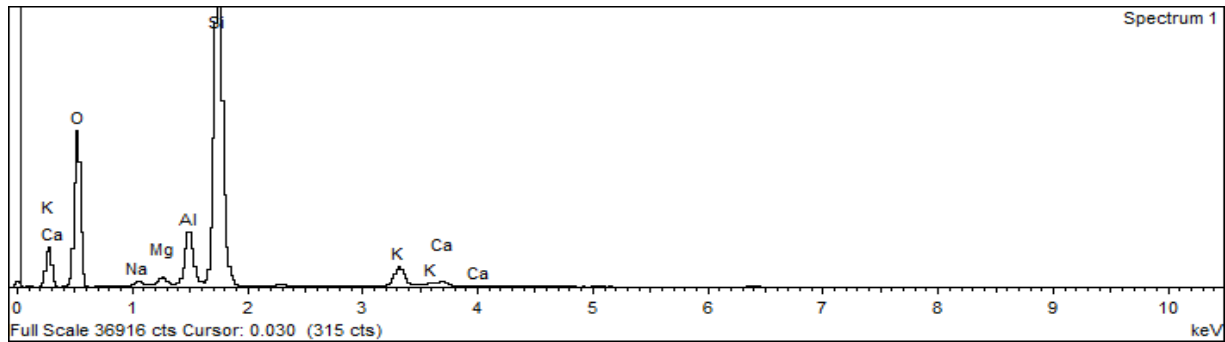
Figure SI1.4.1 Nitrogen adsorption isotherms in the commercial FER and FER-GHA zeolite samples.

The first set of SEM and EDX measurements of the FER-GHA sample were carried out at the Faculty of Science and Engineering, University of Wolverhampton, United Kingdom. A PANalytical Empyrean Powder X-ray diffractometer (PANalytical, Malvern, UK) was used to collect data using Bragg-Brentano geometry and a slit configuration of a degree fixed divergence slit of 0.25° . Using a ZEISS EVO50 scanning electron microscope equipped with Energy Dispersive X-ray analyzer (EDX), the morphology of the starting materials and the as-synthesized zeolites, as well as their chemical compositions, were determined by a Zeiss EVO 500 (Zeiss, Cambridge, UK). Bauxite, kaolin and zeolite powder samples were dry sprayed onto aluminum stubs using double-sided adhesive carbon discs. They were then coated with gold to decrease static charging during their observation under SEM conditions.

An analogous procedure was repeated at the University of Bath for both the commercial and FER-GHA samples. The EDX and other images were taken on an Hitachi SU3900 variable pressure SEM with attached Oxford Instruments 170 mm² Ultim Max EDX detector. Samples were coated with 10 nm of Gold for imaging and uncoated in low vacuum for EDX. The high resolution FE-SEM images were taken on a Jeol JSM-7900F FE-SEM. The surface area of each of the samples was determined at the.

SEM and EDX Spectra of FER-GHA

Spectra are of the H-FER form of the FER-GHA zeolite following the complete synthesis in section SI1.0.0.



Spectrum processing :

Peaks possibly omitted : 2.289, 6.388, 8.018 keV

Processing option : All elements analyzed (Normalised)

Number of iterations = 4

Standard :

O SiO₂ 1-Jun-1999 12:00 AM

Na Albite 1-Jun-1999 12:00 AM

Mg MgO 1-Jun-1999 12:00 AM

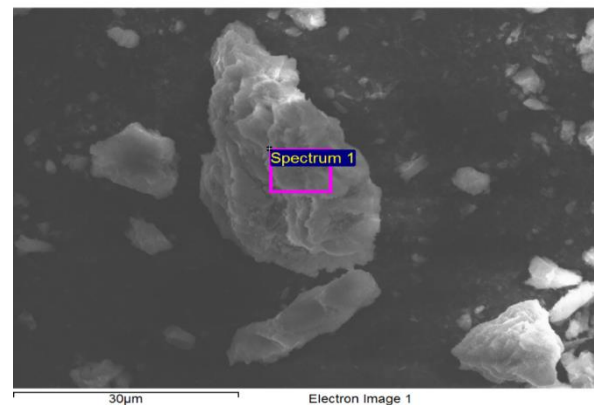
Al Al₂O₃ 1-Jun-1999 12:00 AM

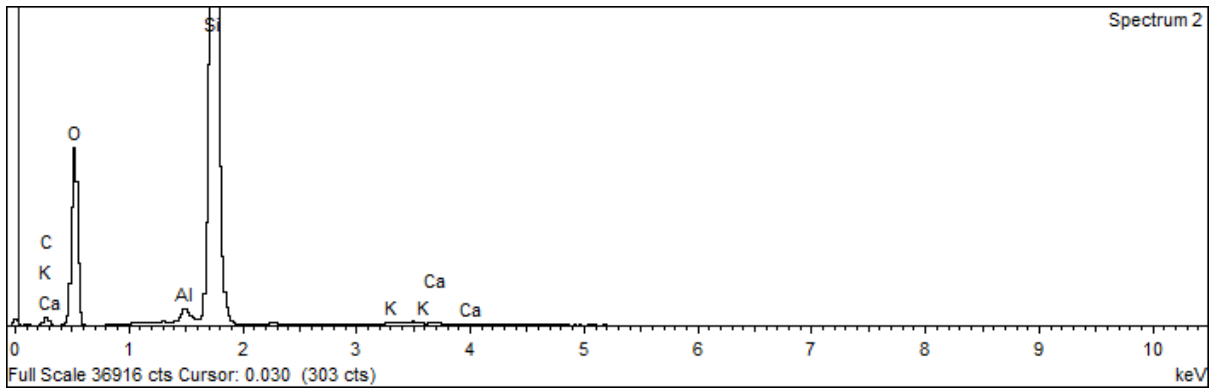
Si SiO₂ 1-Jun-1999 12:00 AM

K MAD-10 Feldspar 1-Jun-1999 12:00 AM

Ca Wollastonite 1-Jun-1999 12:00 AM

Element	Weight%	Atomic%
O K	55.42	68.90
Na K	0.61	0.53
Mg K	0.79	0.65
Al K	5.02	3.70
Si K	34.22	24.24
K K	3.15	1.60
Ca K	0.78	0.39
Totals	100.00	





Spectrum processing :

Peaks possibly omitted : 1.040, 2.268 keV

Processing option : All elements analyzed (Normalised)

Number of iterations = 6

Standard :

C CaCO3 1-Jun-1999 12:00 AM

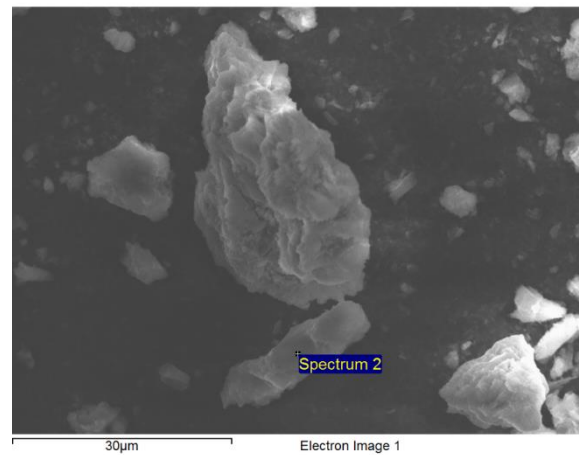
O SiO2 1-Jun-1999 12:00 AM

Al Al2O3 1-Jun-1999 12:00 AM

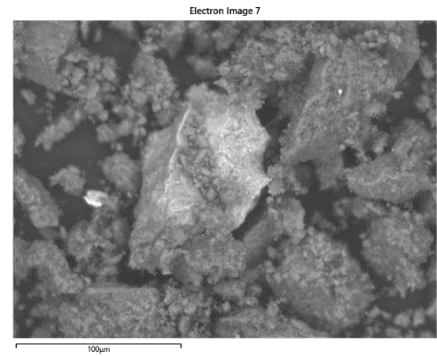
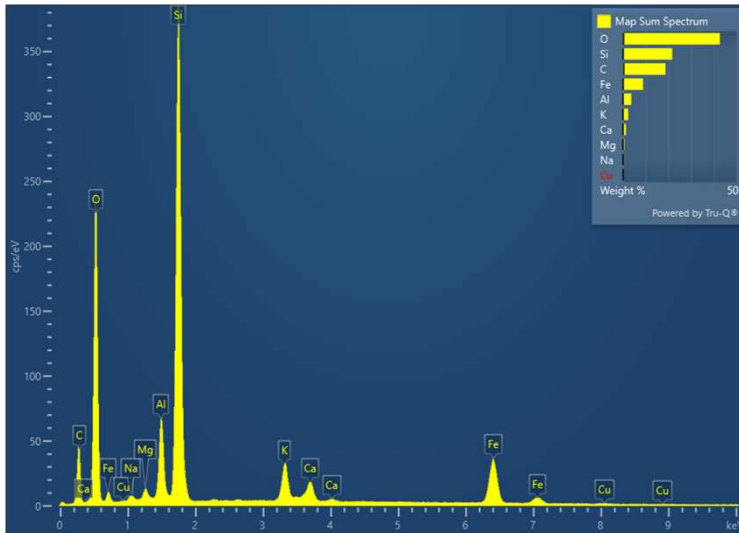
Si SiO2 1-Jun-1999 12:00 AM

K MAD-10 Feldspar 1-Jun-1999 12:00 AM

Ca Wollastonite 1-Jun-1999 12:00 AM



Element	Weight%	Atomic%
C K	12.70	19.28
O K	49.08	55.96
Al K	0.74	0.50
Si K	37.05	24.06
K K	0.18	0.09
Ca K	0.25	0.11
Totals	100.00	



Map Sum Spectrum					
Element	Line Type	Apparent Concentration	Wt%	Wt% Sigma	Atomic %
C	K series	39.54	18.68	0.35	28.75
O	K series	174.99	42.60	0.22	49.21
Na	K series	1.88	0.35	0.03	0.28
Mg	K series	3.93	0.54	0.02	0.41
Al	K series	33.42	3.63	0.04	2.49
Si	K series	226.19	21.62	0.12	14.23
K	K series	22.05	2.24	0.03	1.06
Ca	K series	17.36	1.29	0.03	0.60
Fe	K series	100.17	8.81	0.08	2.92
Cu	K series	2.54	0.23	0.05	0.07
Total:			100.00		100.00

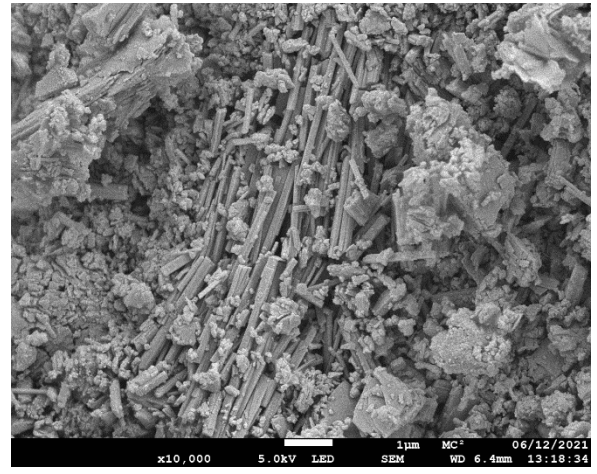
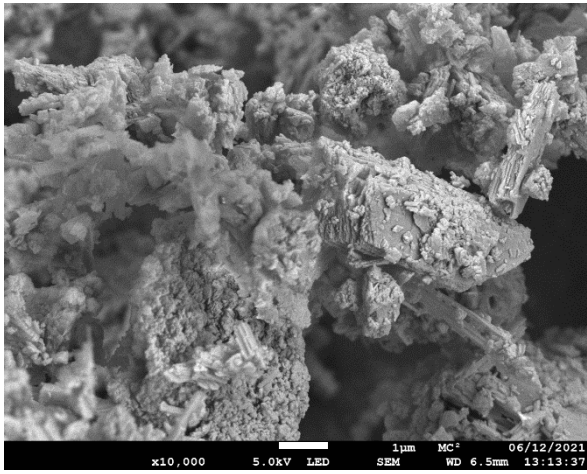
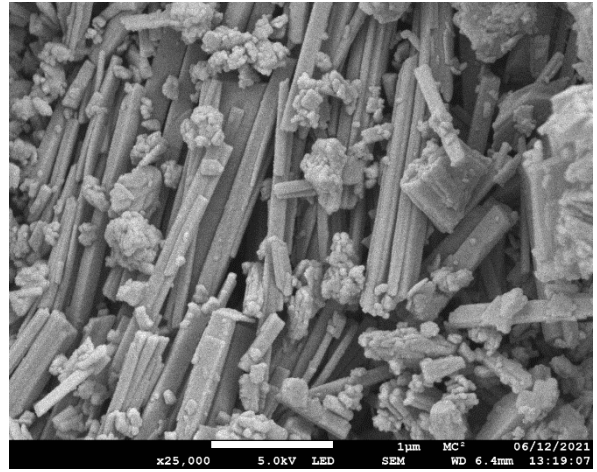
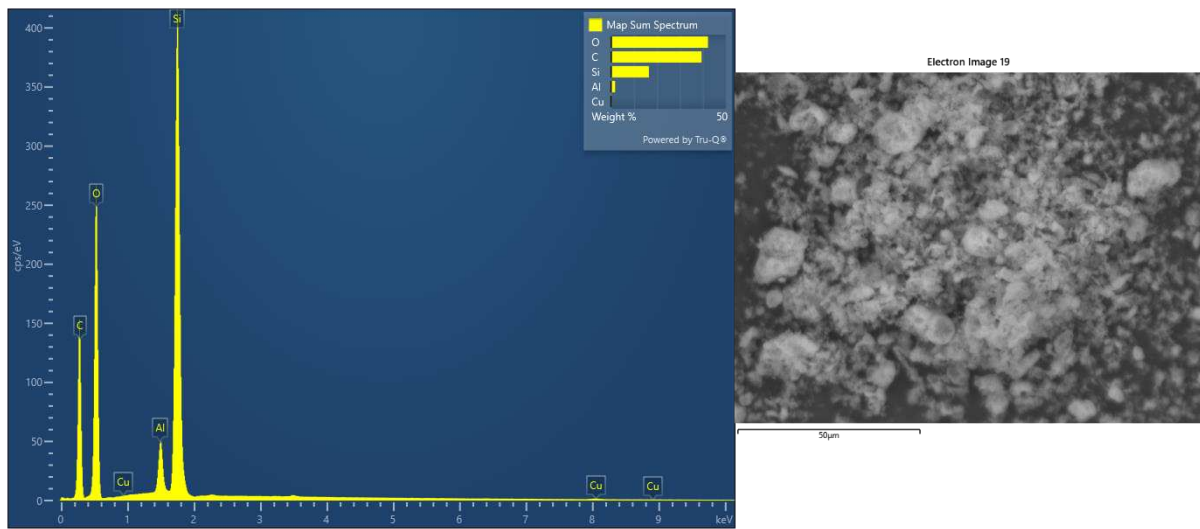


Figure S11.4.2 SEM images of the FER-GHA sample.

SEM and EDX Spectra of commercial FER

Spectra are of the commercial H-FER(10) sample from Zeolyst International (CP914C).



Map Sum Spectrum					
Element	Line Type	Apparent Concentration	Wt%	Wt% Sigma	Atomic %
C	K series	141.36	39.38	0.09	49.91
O	K series	175.18	42.19	0.09	40.14
Al	K series	21.77	1.75	0.01	0.99
Si	K series	231.14	16.44	0.04	8.91
Cu	K series	3.08	0.23	0.02	0.06
Total:			100.00		100.00

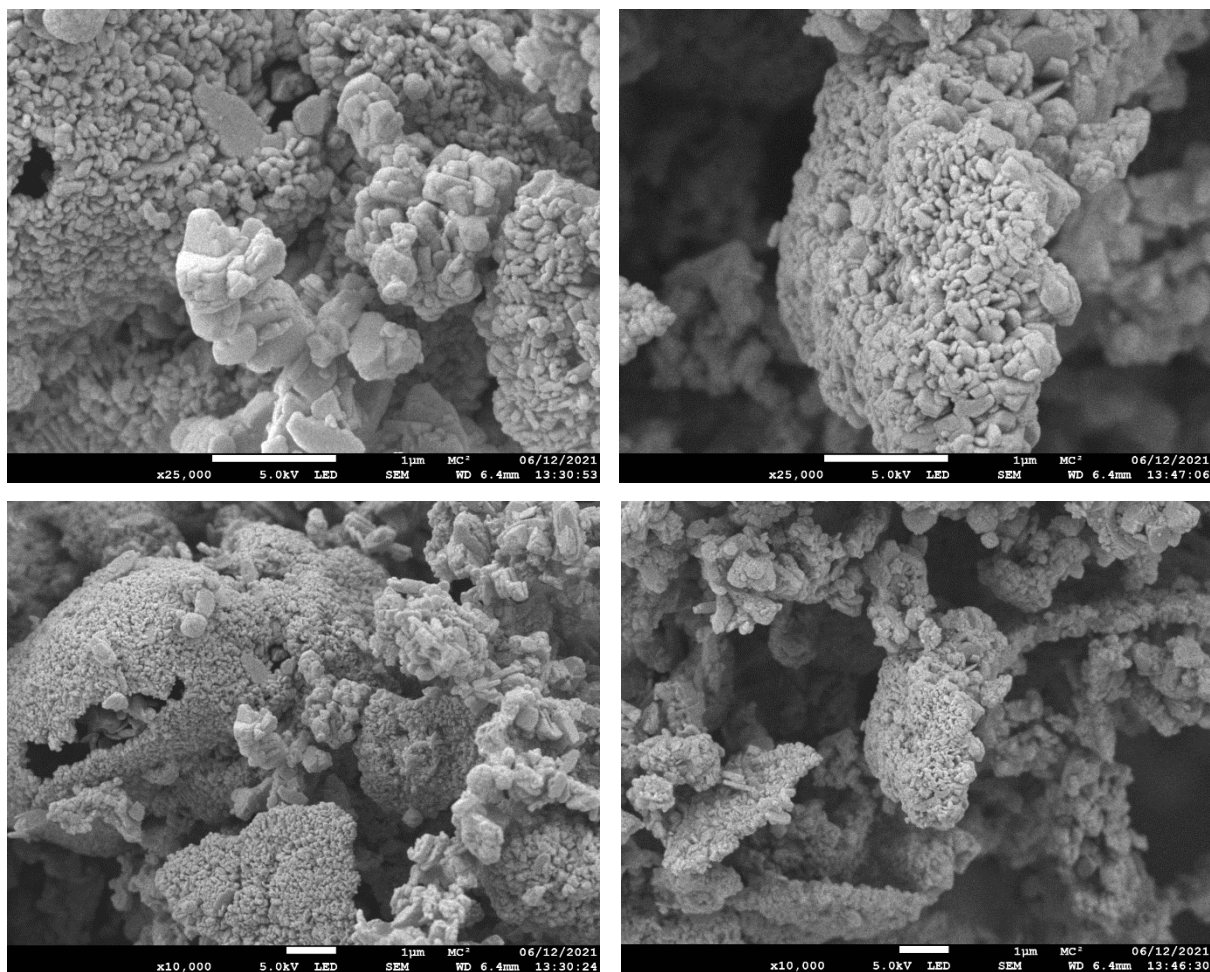


Figure S11.4.3 SEM images of the commercial FER sample.

Both the commercial and FER-GHA EDX spectra are dominated by signals from the Si, Al and O within the samples as expected from any zeolites. Signals from C are present due to the adhesive carbon tabs on which the sample is placed and can be disregarded. The commercial sample shows very small traces of Cu whilst the FER-GHA shows the presence of multiple cations such as K (< 3 wt%), Na, Mg, Ca (< 1.3 wt%) and potentially a large amount of Fe (< 9 wt%). The slight traces of copper noted in the commercial sample are unexpected. Copper is not a known component of commercial ferrierite, nor do we believe it is employed in the synthesis of said material. This signal may be an artefact but is also plausibly a contaminant.

The FER-GHA sample, imaged in figure S11.4.2, shows multiple different morphologies as shown in the high-resolution SEM images, and thus a reliable crystallite size distribution could not be established to measure the average crystallite size. The commercial FER sample shows much more regular crystallite size distribution, imaged in figure S11.4.3, and thus measurement and calculation of the average crystallite size was possible giving an average diameter of ~97 nm.

SI 1.5 Diffraction characterisation of zeolite samples

Upon cooling to a base temperature (~ 6 K), a diffraction pattern from the empty zeolites was obtained alongside the QENS spectra, shown in figure S11.5.1³. While the bulk structures are consistent, some differences are notable. Diffraction peaks observed in the commercial sample are seen in the FER-GHA zeolite however many are shifted to a slightly higher d-spacing – particularly noticeable in the two intense peaks between 3.4 – 3.6 Å. Clear additional peaks are seen in the 3.2 – 3.4 Å region – indicating an extra phase within the FER-GHA. The peak shift can be explained by the incorporation of some larger cations, such as calcium and potassium seen in the elemental analysis (found in supplementary information 1.5), within the FER-GHA sample.

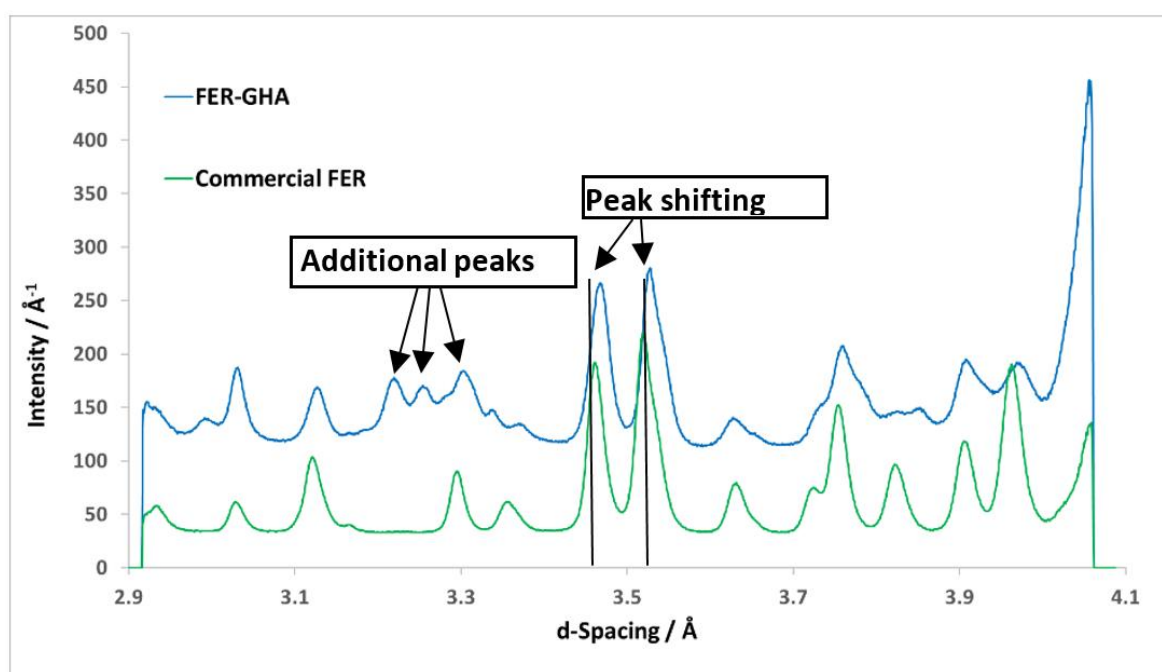


Figure S11.5.1. Neutron diffraction patterns of Commercial and FER-GHA samples.

The powder XRDs were collected using an STOE STADI P double setup with Mythen detectors using Cu-K_{α1} radiation. X-ray diffraction patterns were collected of both samples alongside ZSM5(140) – figure 1.5.2. – using. Both samples are confirmed to be ferrierite. We now examine the FER-GHA sample in more detail. The broad shoulder at 20-25° 2θ suggests that amorphous silica is present in this sample – potentially unreacted from the synthesis. The broadness of peaks, and therefore reduced intensity across the whole pattern, show that this sample is less crystalline than the commercial sample as well as slight peak-shifting due to the incorporation of larger cations into the framework such as Ca²⁺ and K⁺ instead of H⁺ in the case of the commercial FER. Verified synthesis⁴ suggest that the competing phases when synthesising FER are MOR and MFI. Characteristic peaks⁵ from both MOR (6.51°) and MFI (7.94°) are missing – providing no evidence that either structure is present as intergrowths within the sample. The additional peaks observed are likely from impurities.

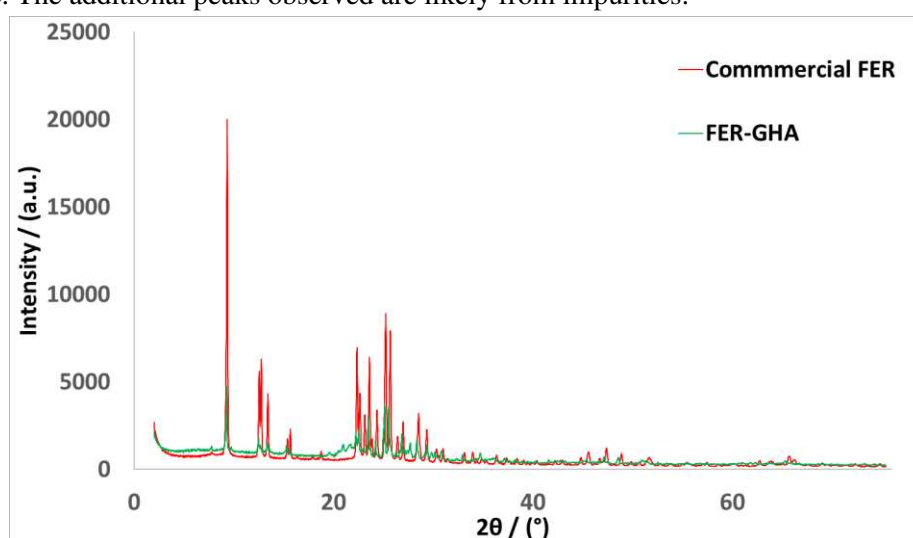


Figure 1.5.2. X-ray diffraction patterns of commercial FER and FER-GHA.

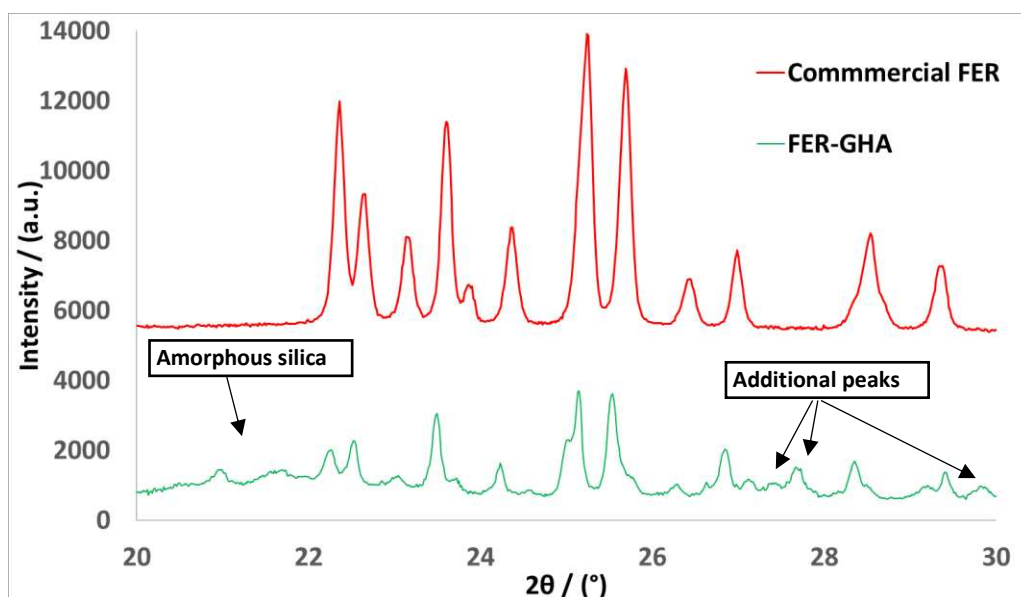


Figure 1.5.3. X-ray diffraction patterns of commercial FER and FER-GHA. Only 20-30° 2θ is shown. Commercial FER pattern is offset by 5000 a.u. for clarity. Annotations included for detail.

QENS fitting and analysis

In the section, the additional QENS spectra and their corresponding fits are shown alongside the EISFs and FWHM which pertain to these fits.

SI 1.6 EISF fitting

Rotation can be characterised by fitting a range of different models – figure 1.6.1– to the EISF.

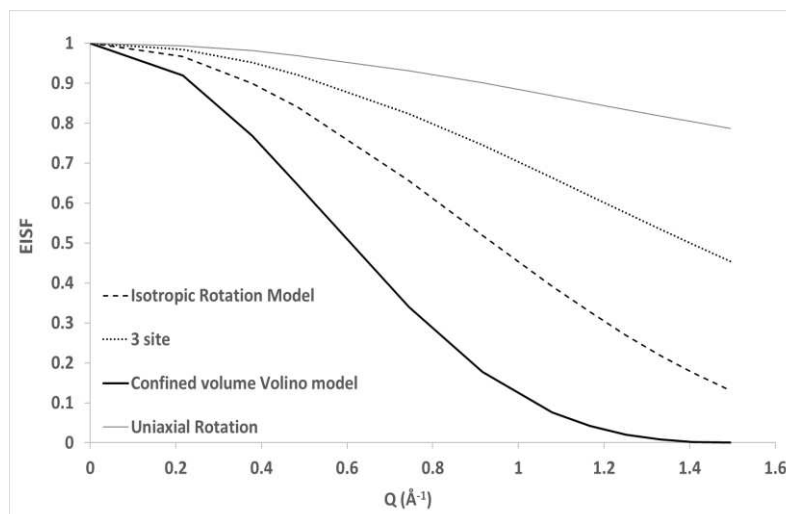


Figure SI1.6.1. Examples of EISF models and their behaviour which may be used for characterising rotation.

The isotropic rotation model describes rotation whereby the methanol molecule has no average orientation – pictured in figure 1.6.2. The isotropic rotation of a methanol molecule has a radius of 1.48 Å and is plotted as such in figure 1.6.1. Where the EISF follows the relationship:

$$A_0(Q) = j_0^2(Qr) \quad (7)$$

where r is the radius of rotation and j_0 is the 0th order spherical Bessel function:

$$j_0(Qr) = \frac{\sin(Qr)}{(Qr)} \quad (8)$$

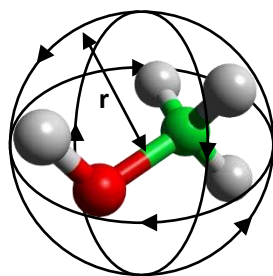


Figure SI1.6.2. Schematic of a methanol molecule rotating isotropically within a radius of rotation ‘ r ’

The next two models describe a molecule that is only rotating on one axis, either as a continuous motion or as a ‘jump’ rotation to several sites. In the case of a rotating methanol molecule, depicted in figure

1.6.3, a three-site jump or uniaxial model can be used to describe the rotation of the methyl group. This may occur if the molecule is immobilised via strong bonding through the hydroxyl group to a zeolite acid site. Both of these rotations will have radii of 1.01 \AA – giving the EISFs shown in figure 1.6.1 – which relates to the radius of the rotor formed of a methyl group.

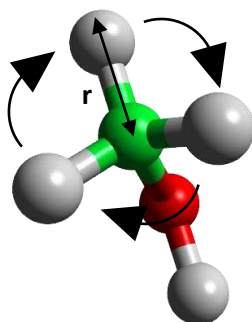


Figure SI1.6.3. Schematic of a methanol molecule rotating around a fixed axis with a radius of rotation r

In the case of three site rotation of radius r the EISF is given as:

$$A_0(Q) = \frac{1}{3} [1 + 2j_0(Qr\sqrt{3})] \quad (3.3.16)$$

The molecule may also be described by almost continuous rotation, around the same axis, known as uniaxial rotation. This is given by a large number of small jumps to match continuous rotation more closely. The EISF for uniaxial rotation of N jumps is given by:

$$A_0(Q) = \frac{1}{N} \sum_{n=1}^N j_0(Qr_n) \quad (3.3.17)$$

Where r_n is:

$$r_n = 2r \sin\left(\frac{n\pi}{N}\right) \quad (3.3.18)$$

Particles may also be trapped within a confined volume inside a material e.g. a pore or cage. In this case, the diffusion of particles is modelled as being in a localised potential sphere, pictured in figure 1.6.4.

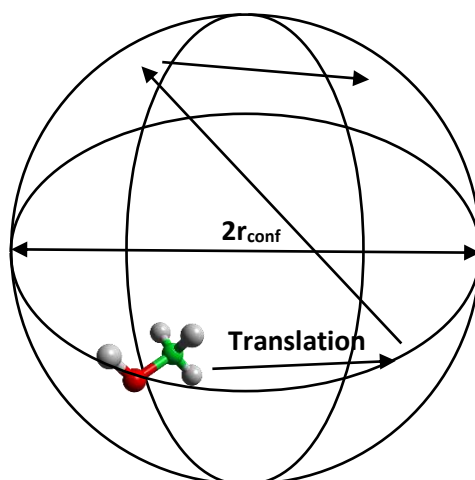


Figure S11.6.4. Schematic of a methanol molecule translating within a confined spherical volume of radius

Volino and Dianoux⁶ developed a model to describe this case where a molecule is translating within a confined volume with radius r_{conf} :

$$A_0(Q) = \left[\frac{3j_1(Qr_{conf})}{Qr_{conf}} \right]^2 \quad (3.3.19)$$

Where j_1 is a Bessel function of the first kind:

$$j_1(Qr_{conf}) = \frac{\sin(Qr_{conf})}{(Qr_{conf})^2} - \frac{\cos(Qr_{conf})}{(Qr_{conf})} \quad (3.3.20)$$

This model is plotted as a function of the radius 3.0 Å in the EISF plot in 1.6.1.

SI 1.7 QENS fits

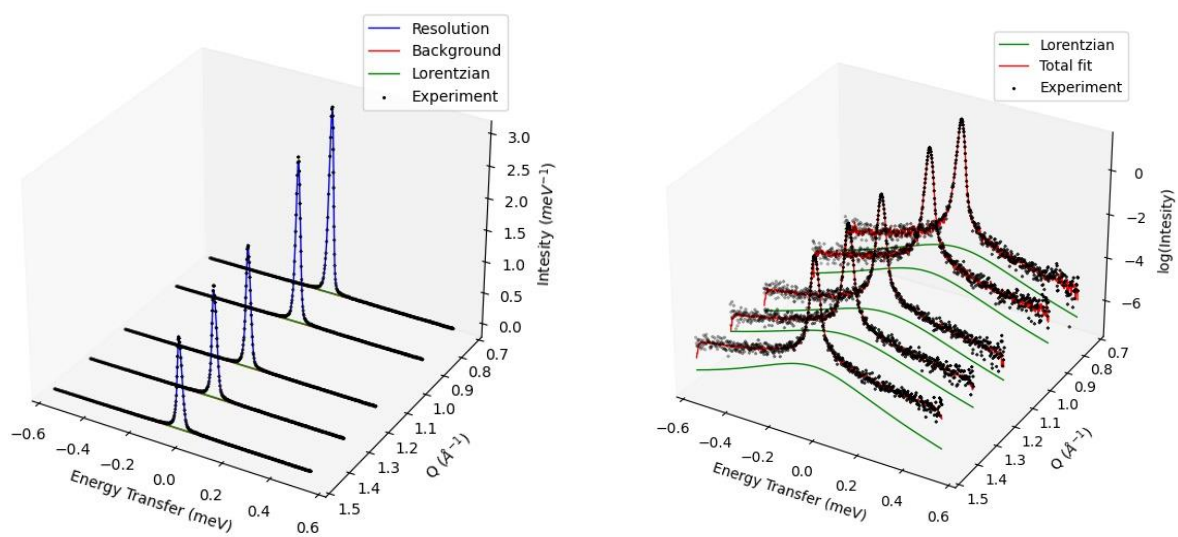


Figure S11.7. Subtracted QENS spectra of 7.34 wt% methanol loaded commercial FER at 273K at $Q = 0.74, 0.91, 1.16, 1.33,$ and 1.49 \AA^{-1} . Left hand plot shows raw intensity, right hand shows log intensity. Selected spectra shown for clarity.

SI 1.8 EISF fits

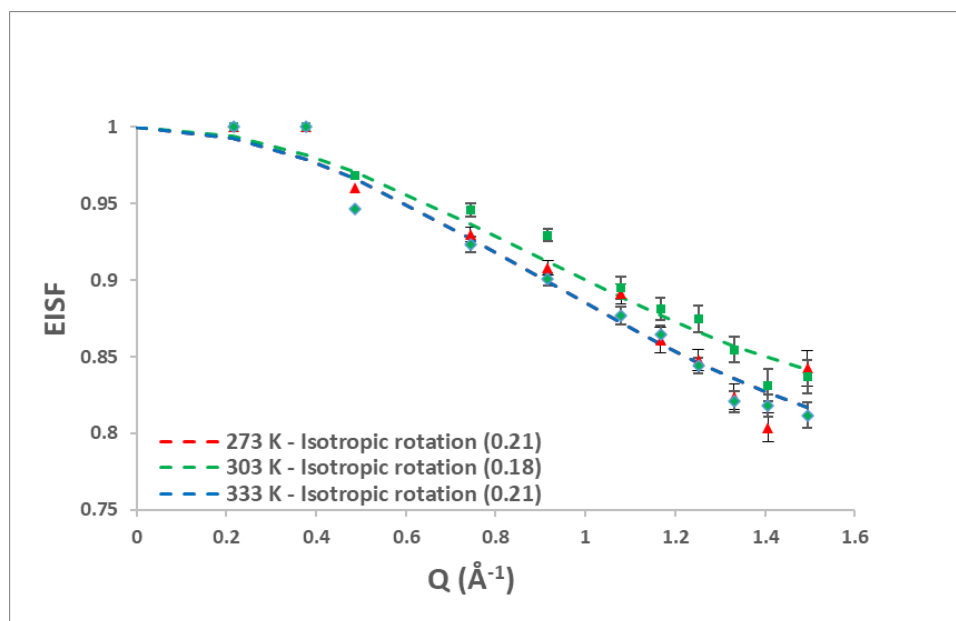


Figure S11.8. Experimental EISF plots for methanol in the 7.34 wt% methanol loaded commercial at 273 K, 303 K and 333 K as well as the fit of the isotropic rotation model with their commensurate mobile fractions.

SI 1.9 FWHM fits

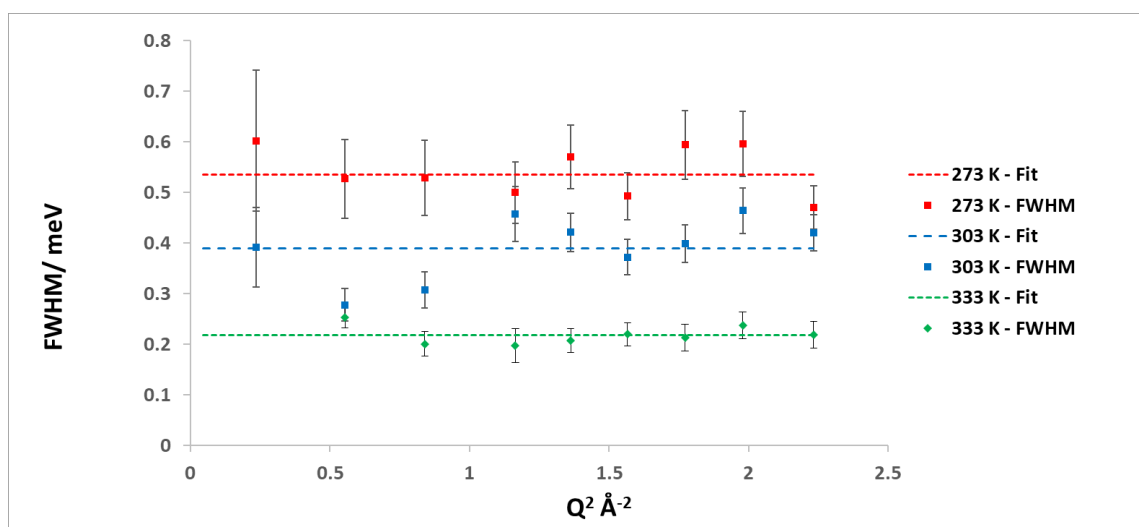


Figure SI1.9.1. Q²-dependence of the FWHM of the Lorentzian component for the 7.34 wt% methanol loaded commercial FER sample at 273 K, 303 K and 333 K. The dotted lines indicate a line of best fit.

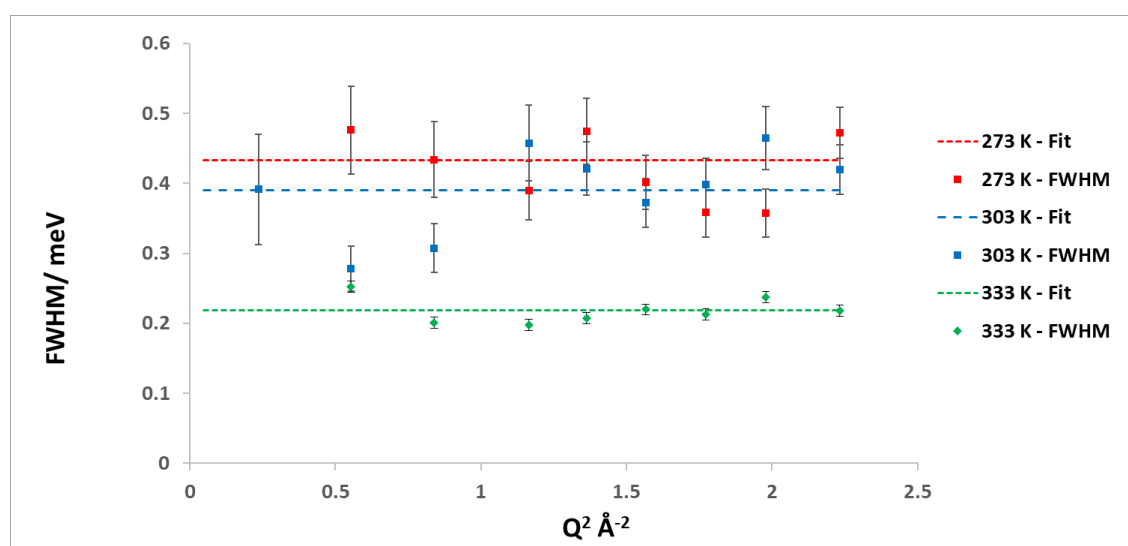


Figure SI1.9.2. Q²-dependence of the FWHM of the Lorentzian component for the 10.18 wt% methanol loaded FER-GHA sample at 273 K, 303 K and 333 K. The dotted lines indicate a line of best fit.

MD simulation analysis

The current section provides information on the analysis of the molecular dynamics simulation.

SI 1.10 BAS-Methanol coordination

Figure SI 1.10 shows an RDF illustrating the interaction between the hydroxyl oxygen of the methanol and the proton of the BAS. At all three temperatures, a sharp peak is seen at approximately 2.75 Å, illustrating the strong interactions between the sorbate and the acid site. Again, the intensity of this peak reduces as the temperature is raised due to the increased movement of the methanol molecules. This is further revealed in figure 6b which shows a snapshot of this interaction from within the simulation. The proximity of the peak indicates that this is the strongest interaction between the framework and the methanol, and thus the major driving force for the slowing of the methanol molecules.

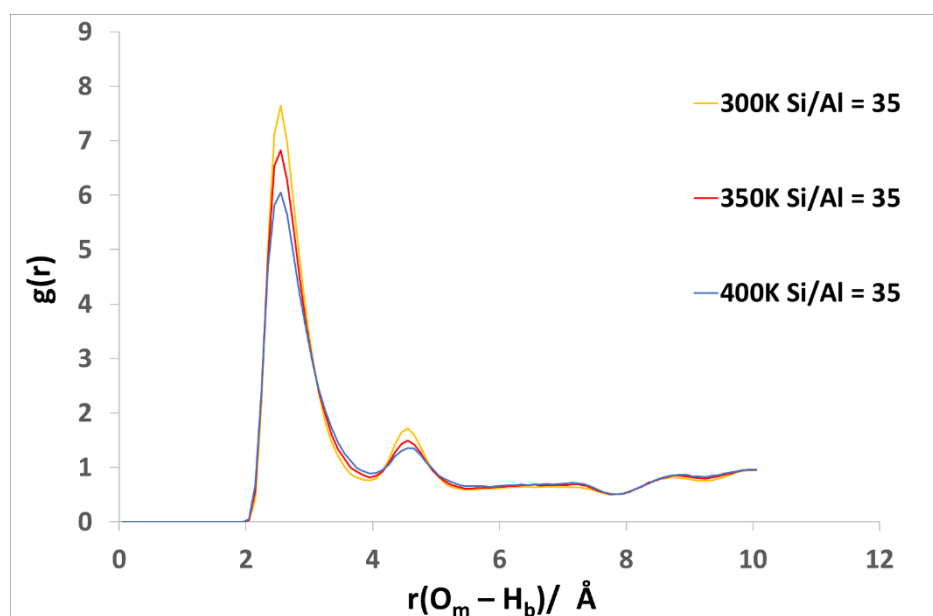


Figure SI1.10. RDF between the methanol hydroxyl oxygen and hydrogen of the Brønsted acid site in the siliceous cells or Si/Al = 35 cells, at 300 K, 350 K and 400 K.

SI 1.11 Intermediate scattering function fitting

The exponents of the intermediate scattering function (ISF) fitting Γ one and two are equivalent to the FWHM which may then be used to calculate the rotational diffusion coefficients of each motion by examining its Q^2 dependence. The resulting rotational diffusion coefficients are in the order of $1 \times 10^{10} \text{ s}^{-1}$ and $1 \times 10^{12} \text{ s}^{-1}$, respectively. The value of Γ_2 lies above the present experimental window of 0.55 meV. This is clearly observable in figure SI1.11 where the second exponential falls rapidly, beyond the experimental timescale. This may be related to motions which are too fast to be observed by the spectrometer such as the rotation of the methanol O-H proton around the C-O axis.

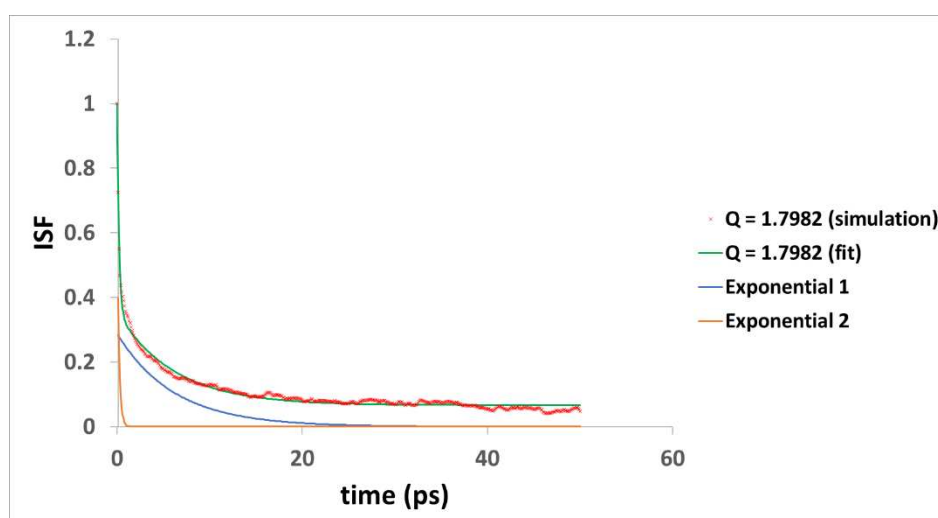


Figure SI1.11. ISF fit at $Q = 1.8$ of the 300 K Siliceous system, showing the combined total fit and the individual exponential functions.

References

1. E. Dempsey, *Journal of Catalysis*, 1977, **49**, 115-119.
2. E. G. Brandt and A. P. Lyubartsev, *The Journal of Physical Chemistry C*, 2015, **119**, 18110-18125.
3. M. T. Telling and K. H. Andersen, *Physical Chemistry Chemical Physics*, 2005, **7**, 1255-1261.
4. in *Verified Syntheses of Zeolitic Materials*, eds. H. Robson and K. P. Lillerud, Elsevier Science, Amsterdam, 2001, pp. 167-168.
5. in *Collection of Simulated XRD Powder Patterns for Zeolites*, eds. M. M. J. Treacy, J. B. Higgins and J. B. Higgins, Elsevier Science B.V., Amsterdam, 2001, pp. 7-13.
6. F. Volino and A. Dianoux, *Molecular Physics*, 1980, **41**, 271-279.